Journal of Process Control 162 (2026) 103725

Contents lists available at ScienceDirect

Journal of Process Control

journal homepage: www.elsevier.com/locate/jprocont

Part-mass control in injection molding of recycled thermoplastics by learning-enabled model predictive cavity-pressure control

Jens Ahlers [a,*], Robert Göllinger [a,*], Moritz Mascher [b], Christopher Schulte [a], Philipp Schubert [a], Christian Hopmann [b], Heike Vallery [a,c], Sebastian Stemmler [a]

[a] Institute of Automatic Control, RWTH Aachen University, Campus-Boulevard 30, 52074 Aachen, Germany
[b] Institute for Plastics Processing, RWTH Aachen University, Seffenter Weg 201, 52074 Aachen, Germany
[c] Faculty of Mechanical Engineering, TU Delft, Mekelweg 2, 2628CD Delft, The Netherlands

ARTICLE INFO

Keywords:
Injection molding
Post-Consumer-Recycled Thermoplastics
Cavity-pressure control
Nonlinear model predictive control
Learning-enabled control

ABSTRACT

Post-Consumer-Recycled (PCR) thermoplastics exhibit inconsistent material properties across batches due to impurities and material degradation. Achieving consistent part-quality attributes in processing different batches of PCR requires continuous adjustment of the state-of-the-art injection molding process.

In our work, we present a learning-enabled nonlinear model predictive controller (NMPC) for cavity pressure that updates its model after each injection molding cycle, combined with a learning-enabled part-mass controller that serves as its reference generator. Within the NMPC, we use a physics-based model of ordinary nonlinear differential equations. The model parameters are updated between each injection molding cycle using a sequential quadratic programming approach. We incorporate constraints into the NMPC to prevent issues such as cavity-pressure peaks. The model used inside the part-mass controller is a Gaussian process regression model that leverages a cycle-variant kernel function to account for varying material properties.

We test the proposed control algorithm on a plate-mold geometry, processing both virgin polypropylene and multiple batches of PCR material. While transitioning between virgin and two PCR batches over 50 production cycles without interrupting the injection molding process, the NMPC model and the cavity-pressure reference are automatically adjusted, maintaining a mean part-mass deviation of 0.21 % relative to the part-mass reference. The results show strong potential for automated process-model adaptation and part-mass control when transitioning between virgin material and different PCR batches.

1. Introduction

1.1. Future topics in injection molding

The injection molding (IM) process offers high efficiency, the ability to produce complex plastic parts with high precision, and a high potential for automation [1]. Consequently, the IM industry contributed significantly to the sustained growth of global plastics production after 1950 [2]. Today, worldwide plastic production exceeds 400 million tons per year, with IM among the predominant manufacturing processes [2].

In response to growing environmental concerns, a more sustainable approach to plastics processing is imperative. Accordingly, the European Union's Green Deal calls for a 50 % reduction in the use of virgin plastics by 2030 [3]. The evolving legislative landscape puts pressure on manufacturers to integrate PCR polymers into their existing production processes [4]. At the same time, the industry is shifting towards digitization and smart manufacturing. According to [4,5], the most emerging trends in plastics processing for 2025 and beyond are "smart manufacturing and AI-driven automation" and "biodegradable and recyclable plastics".

The material properties of plastic granules change during the recycling process due to polymer degradation and impurities introduced to the material during recycling [6]. Additionally, regional and temporal changes in consumer behavior alter the composition of PCR materials. As a result, different batches of PCR material exhibit different behavior during IM. According to [6], the melt flow rate (MFR) can rise up to 45 % compared to the virgin material, indicating a substantial decrease in melt viscosity of the processed PCR material. These variations result in inconsistent quality attributes of the molded parts, leading to rejects and, consequently, being detrimental to the economics of sustainably produced plastics. Yet, current IM technology is not well-equipped to process PCR materials, as batch fluctuations yield a wider

* Corresponding authors.
E-mail addresses: j.ahlers@irt.rwth-aachen.de (J. Ahlers), r.goellinger@irt.rwth-aachen.de (R. Göllinger).

https://doi.org/10.1016/j.jprocont.2026.103725
Received 19 November 2025; Received in revised form 13 March 2026; Accepted 6 April 2026
Available online 16 April 2026

range of process conditions. Hence, the reproducibility of both process and part quality is worse than that of IM processing virgin material.

Data-driven approaches to process control are promising to resolve the challenges posed by fluctuating material properties. However, to our knowledge, a control strategy that achieves reproducible part-quality attributes while maintaining a tightly controlled IM process using PCR remains lacking.

1.2. Process control

The most common process-control strategy for injection molding is to switch between two different controlled variables depending on the IM phase. In the injection phase, the screw velocity is controlled, whereas in the packing phase, the screw-antechamber pressure is the controlled variable. Both variables should ensure reproducible process trajectories, but only hold indirect information about the mold inside the part cavity. Furthermore, determining the optimal switchover point is a challenging task that remains an intensively studied topic [7,8]. Suboptimal switchover points can damage the IM mould and degrade part quality. The problem of finding suitable switchover points is highlighted when processing PCR, as the optimal switchover point may differ between material batches.

To adapt the conventional process-control strategy to processing PCR, manufacturers of injection molding machines have incorporated initial adaptation approaches into their latest generation of injection molding machines [9]. KraussMaffei Technologies GmbH (Munich, Germany) offers its process-control software under the name APC plus. In this approach, the melt viscosity during the injection phase of the cycle is compared to a reference cycle to adapt the switchover point and the holding pressure between production cycles [10]. Recent injection molding machines by ENGEL AUSTRIA GmbH (Schwertberg, Austria) use their process-control software iQ weight control. In comparison to APC plus, iQ weight control adapts the switchover point within the cycle and considers limits to the switchover point and holding pressure during the adaptation process. While introducing adaptation capabilities, both products require a reference cycle for comparison [11], which implies manual setup effort and restricts generalization. Also, neither approach offers closed-loop control of cavity-related quantities that are more directly related to part quality [12].

An approach that circumvents the problem of defining a suitable switchover point is controlling the cavity pressure throughout the cycle. Cavity pressure correlates strongly with different quality attributes of the molded part [13], thereby making it a natural choice for a controlled variable. This approach is referred to as phase-unifying cavity-pressure control. It should be noted that direct control of cavity pressure requires additional sensors in the mold, which to this day are not considered industry standard.

In this context, our research group presented a phase-unifying model predictive controller (MPC) that allows tracking predefined cavity-pressure Refs. [14]. To compensate for unknown material or process dynamics, the underlying process model is updated throughout the current cycle by an observer design for parameter estimation. In [15], an unscented Kalman filter (UKF) is investigated to estimate a lumped parameter for the pressure build-up equation within the mold. However, the information about the dynamic behavior of the parameter is not reused in subsequent cycles. Moreover, a single parameter seems inadequate to map the various effects of PCR batch fluctuations.

Prior work [16] also includes a norm-optimal iterative learning controller (NOILC) for cavity-pressure control that promises extended adaptation capabilities compared to an MPC. The controller updates the input trajectory between IM cycles based on previously observed process trajectories. However, the NOILC acts as a feedforward controller during the IM cycle, making it prone to abrupt model mismatch, e.g., after batch changes, and thus less suitable for PCR processing. Choosing suitable adaptation gains furthermore constitutes an open research question.

Similar to the NOILC, there are also MPC implementations that exploit the repetitive nature of batch processes. As outlined in [17], the approaches can be categorized into three groups:

1. Learning on Control Input,
2. Learning on Model Parameter, and
3. Learning on Tracking Reference.

The first group of learning-based MPCs can be characterized by controllers that learn a correction term for the control input based on previous cycles, similar to the NOILC approach, but within an MPC framework called Iterative Learning MPC (ILMPC). In [18], the authors introduce a terminal-constrained robust ILMPC and demonstrate its application to the thermoplastic IM process on the conventional control strategy in simulation. The implementation relies on a two-dimensional system model with time and batch as the dimensions and accounts for switching between different process phases. During runtime, the controller does not need to solve a Quadratic Program. Instead, the control law is calculated offline by solving a min–max optimization explicitly via Linear Matrix Inequalities derived from 2D Lyapunov stability theory. To address the challenges posed by strong nonlinearity and wide setpoint variations in batch processes, the same research group [19] utilizes a model that switches among different linearized operating points. Their control strategy minimizes unnecessary conservativeness by using a less conservative controller for normal operations and switching to a robust, fault-tolerant controller only when actuator faults occur. While this group of methods offers a simpler approach to stability guarantees, they struggle to handle frequent variation in the reference across batches [17].

A second category of learning-based MPC methods addresses the challenge of batch-varying references by learning the underlying MPC model parameters, rather than applying a residual correction to the previous batch's control input trajectory. This approach exhibits a fast convergence rate, yet it makes stability analysis challenging and is susceptible to structural model mismatches [17].

The third category modifies the reference trajectory instead of the controller itself. While this maintains the original MPC framework, it remains susceptible to the same problems inherent to methods that learn on the control input [17].

To mitigate the impact of material property changes on quality attributes, the controller's reference must be adjusted accordingly from batch to batch. Additionally, the system's quantitative dynamic behavior fluctuates and is initially unknown. Both points make learning the underlying NMPC model parameters a reasonable choice for processing PCR.

1.3. Control of quality attributes

PCR batch fluctuations call for direct quality-attribute control. While in general, different part-quality attributes can be considered, the industrial standard is the part mass.

In [16], the authors apply a virgin material model alongside a time-dependent cooling equation and a layered cavity-pressure controller to obtain consistent part weights across IM cycles. The parameters of the cooling equation and the material model must be adjusted for different part geometries and different materials to derive adequate cavity-pressure-reference levels. The control approach furthermore assumes a cycle-invariant plant and material behavior. It is thus ill-suited for PCR processing.

An approach for estimating part mass using the cavity pressure was also proposed in [20]. The authors estimate the part mass using a parametric model, where the integral of the cavity pressure over a cycle serves as the input. This method was validated on polypropylene (PP) and acrylonitrile butadiene styrene (ABS) materials. Generalization to PCR processing is unclear.

Part-mass estimation based on the pressure build-up equation in the screw antechamber and a material model stemming from the Tait equation is presented in [1,21]. The authors then predict the mass flow rate leaving the screw antechamber and entering the mold cavity as part of an MPC to control the part mass [12]. However, no cavity-pressure sensor is used. The approach thus relies on modeling the mass-flow-rate transfer from the screw antechamber to the cavity precisely and thus on an accurate material model. The presented topology is limited to part-mass control and cannot be extended to other quality attributes, such as part dimensionality or gloss.

Last, a PID controller to adjust a setpoint of the nozzle pressure to compensate for mass variations originating from different PCR materials is suggested in [22]. Here, the time required to reach a desired in-mold cavity-pressure value is used as an indicator. The approach is investigated for multiple post-industrial recycling blends with MFR ranging from 5 to 50 g/(10 min). The MFR was measured at a temperature of 230 °C using a test weight of 2.16 kg. Yet, transitioning between batches is not considered. Using a method called "auto viscosity", the same authors report a coefficient of variation for the part mass of under 5 % without directly controlling the cavity pressure [22]. In [23], the research group explores polynomial models and artificial neural networks to predict and generalize to different quality attributes in screw-pressure controlled IM. The authors achieve errors of 5 % for the linear and polynomial models and 10 % for the artificial neural network in part-mass prediction using five different blends of PCR material.

1.4. Limitations of process and quality-attribute control for PCR

The switchover point used in the conventional injection molding process control must be updated continuously. This requires costly manual intervention by the machine operator.

Approaches based on screw-pressure control are believed to be less robust towards PCR batch fluctuations. It appears natural that quantities measured at the origin of the molded part have a stronger influence on the part-quality attributes.

All of the aforementioned cavity-pressure approaches struggle with the changing plant dynamics when transitioning between different batches of PCR material. Accurately parameterizing models for different batches of PCR material via prior material characterization is laborious and costly. Since all of the aforementioned model-based control approaches assume cycle-invariant plant behavior, they do not include a strategy for updating their underlying models.

1.5. Contribution

We consider the following three points as our main contribution.

- C1 Since the underlying control concept requires adapting the cavity-pressure reference during PCR processing, we chose to use an MPC scheme that learns the parameters. Obtaining a process model for an MPC for cavity-pressure control in IM typically requires prior knowledge about the processed material, machine dynamics, and mold geometry, usually necessitating prior experiments. In this work, the controller automates this step by first using a model-free controller to generate experimental data and then learning the plant dynamics from this initial cycle. After learning an initial model of the process, the controller switches from the model-free controller to an NMPC. The NMPC's process model is then updated between each injection molding cycle to mitigate changing plant dynamics.
- C2 We investigate the adaptation capabilities of the learning-enabled NMPC during transitioning between different batches of PCR and virgin material. During the transition between different materials, we do not interrupt the injection molding process. We do not incorporate prior knowledge about the processed materials.
- C3 To close the quality-attribute control loop, we propose and investigate a learning-enabled part-mass controller that can handle unknown batch- and material transitions by collecting measurements of the part mass. The controller can update the underlying cycle-variant part-mass prediction model using the part-mass measurements when available, while giving more weight to more recent measurements.

The remainder of this journal paper is structured as follows: First, we outline the control approach in Section 2. We then proceed with the implementation details of the process model (Section 3), the model optimizer (Section 4), NMPC (Section 5) and the part-mass controller (Section 6). In Section 7, we present the details of the experimental setup used to generate the results described in Section 8 and discussed in Section 9.

2. Control approach

2.1. Overview of the control approach

An overview of the control approach is presented in Fig. 1. In the lower part of Fig. 1, a swim-lane diagram depicts the execution order across individual cycles c for the different elements of the complete control loop. The primary goal is to control the part mass. To achieve this, we divide the control approach into two control loops with different sampling times. The process-control loop (highlighted in blue) controls the cavity pressure p_C with a sample time of 8 ms given a cavity-pressure reference p_C^{ref}. This reference is provided by the part-mass controller and remains constant throughout the execution of the process-control loop. The part-mass controller does not run with Δt, but is executed once between the IM cycles.

2.2. Process control

For the first cycle ($c = 0$), we use a model-free proportional controller (P in Fig. 1). Using the P controller initially allows us to generate identification data to determine the model dynamics. We chose a proportional controller for the first cycle because it is safe and easy to tune. It can be tuned by initially setting a low controller gain and incrementally increasing it until sufficient closed-loop performance is achieved. For this study, we assume that a reasonable value for K_P is already known. Note that model optimization can also be performed during the P controller-tuning phase.

In all subsequent cycles ($c > 0$), we make use of a learning-enabled nonlinear model predictive controller (NMPC) in combination with an extended Kalman filter (EKF). Apart from its enhanced control performance compared to simpler methods, the NMPC can directly incorporate constraints in calculating a suitable controller output. Overshoots in the cavity pressure, for instance, lead to burrs and flashes [24]. The machine's maximum clamping force should not be exceeded. It is also natural to limit the maximum injection velocity, since high injection velocities can lead to material deterioration, depending on the processed material [1,24]. Additionally, the screw should not retract during injection and packing to reduce strain on the screw drive. However, MPC requires a model of the underlying process that can be used for real-time optimization. A model describing the injection molding process is usually nonlinear. For this reason, we use an NMPC.

2.3. Model optimizer

Because the injection molding machine needs time to cool the part, eject it, and dose up new material, there is sufficient time to optimize the model parameters for the next cycle. The model optimizer determines the model parameters $\boldsymbol{\Theta}^*$ from the observations made from the previous injection molding cycle. This model is then used within the NMPC and the EKF during the subsequent production cycle. Our

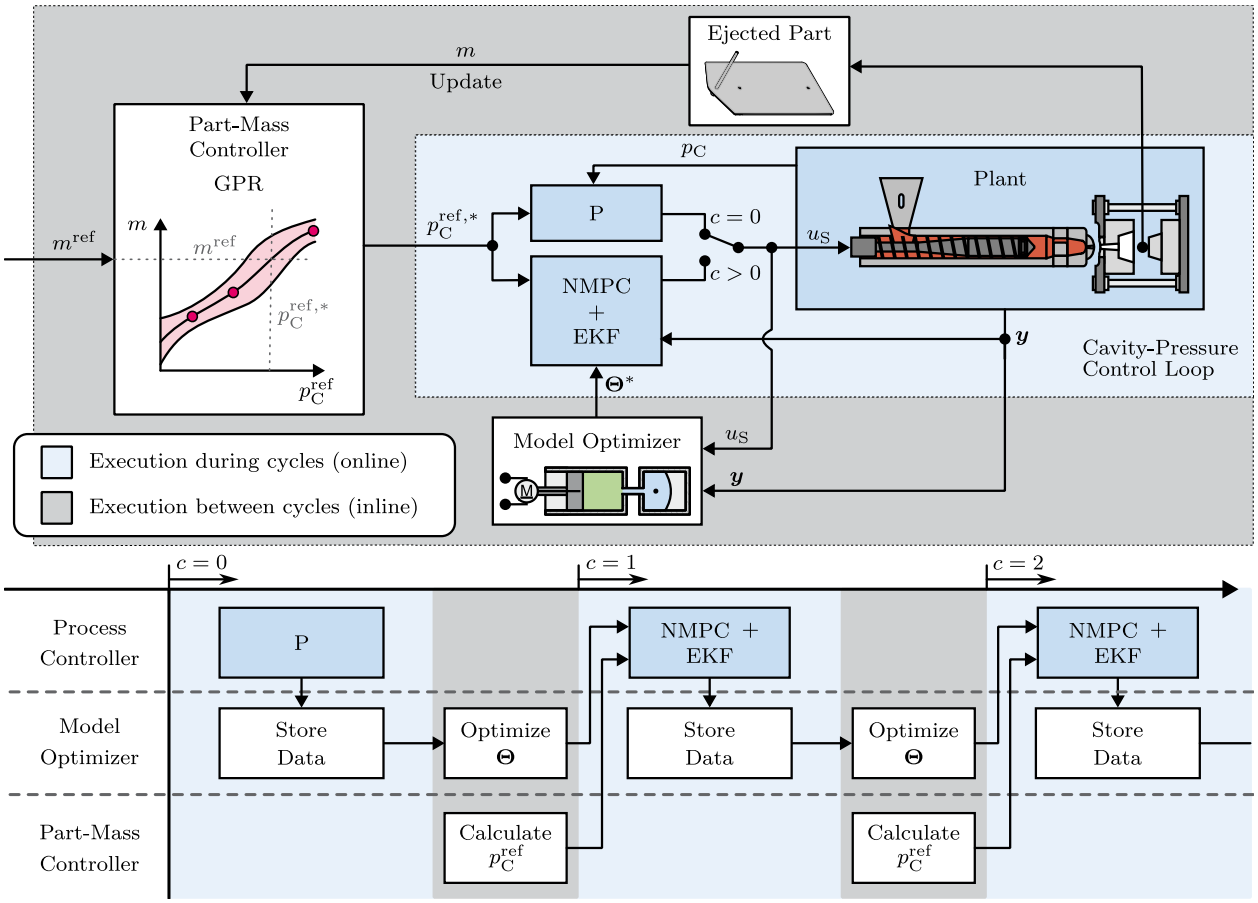

Fig. 1. The control approach consists of algorithms that are executed during the cycles or between them. Between cycles, the model optimizer adapts the process-model parameters used inside the NMPC and EKF. The updated part-mass controller generates a cavity-pressure reference based on the desired part mass. The updated cavity-pressure controller then follows this reference during the cycle.

approach employs a physics-based model to obtain an interpretable model of the process. This enables us to understand how parameters change during the learning process. The physics-based model also has the advantage of incorporating meaningful constraints on the model parameters.

2.4. Control of part mass as quality indicator

The part-mass controller calculates the cavity-pressure reference p_C^{ref} for the next cycle given the desired part mass m^{ref}. Since the relationship between quality attributes and process variables is stochastic, we chose a Gaussian process regression model for the part-mass prediction. We utilize the prediction model to generate a suitable reference for the underlying process-control loop $p_C^{ref,*}$. When new measurements of the part mass are available, the model can be updated. In case no update is available, the controller can act as a feed-forward controller.

3. Process model

3.1. Modeling approach

A computational fluid dynamics model in combination with a detailed material model are necessary to model the IM process accurately. However, due to the need for real-time optimization inside the NMPC and limited knowledge of the PCR material, this approach is infeasible.

Instead, we use a lumped-parameter model to obtain a prediction for the NMPC and the EKF. A schematic and simplified overview of the system is presented in Fig. 2.

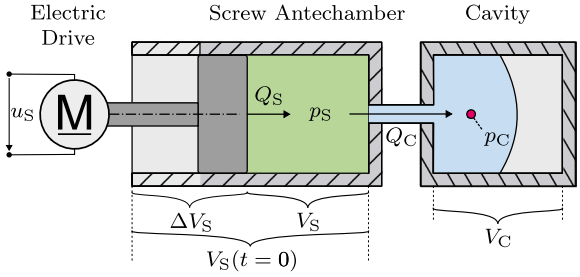

Fig. 2. The modeling approach divides the IM plant into three different submodels: electric drive, screw antechamber, and the cavity inside the mold.

The input to the system is the command signal u_S for the frequency inverter of the servo-electric drive of the injection molding machine. The outputs are the volumetric flow rate Q_S induced by the screw velocity, the screw-antechamber volume V_S, the screw-antechamber pressure p_S, and the pressure p_C measured at the in-mold cavity-pressure sensor location. We divide the complete model into three different submodels.

3.2. Modeling the electric drive

An underlying machine-internal algorithm controls the electric drive of the injection molding machine. The closed-loop behavior is approximated by using a first-order lag element. Herein, we describe the volumetric flow rate induced by the screw velocity using the ordinary

differential equation

$$\frac{\mathrm{d}Q_\mathrm{S}}{\mathrm{d}t} = \dot{Q}_\mathrm{S} = -\frac{1}{T_\mathrm{D}}\left(K_\mathrm{D} u_\mathrm{S} + Q_\mathrm{S}\right), \tag{1}$$

with the time constant T_D and the gain of the linear model K_D. When u_S is negative, the screw moves forward, pushing the molten material into the mold. The volume of the screw antechamber V_S is obtained by integrating

$$\frac{\mathrm{d}V_\mathrm{S}}{\mathrm{d}t} = \dot{V}_\mathrm{S} = -Q_\mathrm{S} \tag{2}$$

over time. Here, Q_S is defined as positive when the screw moves forward, thereby decreasing the volume of the screw antechamber.

Due to the underlying machine-internal control algorithm, we neglect the effect of pressure within the screw antechamber on the acceleration of the machine's electric drive. We assume the underlying drive is sufficiently tightly controlled so that its closed-loop transfer function can be approximated by a first-order lag element. This is typically the case for moderately actuated electric drives. In contrast, as described in [25], accurately modeling the drive dynamics of a servo-pump-driven IM machine necessitates a nonlinear, multi-state approach.

3.3. Modeling the screw-antechamber pressure

For the temporal change in screw antechamber pressure, we utilize the hydraulic pressure build-up equation

$$\frac{\mathrm{d}p_\mathrm{S}}{\mathrm{d}t} = \dot{p}_\mathrm{S} = \frac{K_\mathrm{S}}{V_\mathrm{S}}\left(Q_\mathrm{S} - Q_\mathrm{C}\right), \tag{3}$$

balancing Q_S and the volumetric flow rate Q_C leaving the screw antechamber towards the cavity of the mold. This equation depends on the isentropic bulk modulus, K_S. In Fig. 2, we denote the dosing volume with $V_\mathrm{S}(t=0)$, and the displaced volume with ΔV_S

Using (3), we neglect the thermal effects on the pressure and spatial changes of the pressure inside the screw antechamber. We also assume that there is no flow from the cavity back towards the screw antechamber, or that this flow has the same density as the melt inside the screw antechamber. Furthermore, we assume an ideal sealing behavior of the non-return valve, completely preventing any melt leakage from the screw antechamber to the feed zone of the screw.

3.4. Modeling the cavity pressure

For the cavity inside the mold, we use another pressure build-up equation

$$\frac{\mathrm{d}p_\mathrm{C}}{\mathrm{d}t} = \dot{p}_\mathrm{C} = \frac{K_\mathrm{C}}{V_\mathrm{C}} Q_\mathrm{C} - \dot{S} \tag{4}$$

with the effective bulk modulus K_C, the cavity volume V_C, and a sink term $\dot{S}$ approximating pressure loss due to thermal effects. Since the cavity is not filled from the beginning of the cycle, we must calculate the mixture of the bulk modulus of the plastic and the residual air inside the cavity. The effective bulk modulus also depends on the cavity geometry and is thus specific to the mold. For this reason, we approximate the effective bulk modulus

$$K_\mathrm{C}(\Delta V_\mathrm{S}) = \underbrace{\begin{pmatrix}\psi_1(\Delta V_\mathrm{S}) & \dots & \psi_{N_\psi}(\Delta V_\mathrm{S})\end{pmatrix}}_{\boldsymbol{\psi}(\Delta V_\mathrm{S})^\top \in \mathbb{R}^{1\times N_\psi}} \underbrace{\begin{pmatrix} w_1 \\ \vdots \\ w_{N_\psi}\end{pmatrix}}_{\boldsymbol{w}\in\mathbb{R}^{N_\psi}} \tag{5}$$

with N_ψ functions $\psi_i(\Delta V_\mathrm{S})$ to obtain a flexible representation of the bulk modulus. These functions depend on the volume displaced by the screw

$$\Delta V_\mathrm{S}(t) = V_\mathrm{S}(t=0) - V_\mathrm{S}(t) \tag{6}$$

and are individually weighted with their respective weight w_i. Here, $t = 0$ corresponds to the beginning of the cycle. We use sigmoid functions

$$\psi_i(\Delta V_\mathrm{S}) = \frac{1}{1+\exp\left(a\cdot(r_i - \Delta V_\mathrm{S})\right)} \tag{7}$$

placed equidistantly over the domain of the displaced screw volume, with the center r_i and a common coefficient for the steepness a. Here, i denotes the specific index of the basis function inside the vector $\boldsymbol{\psi}$. In Fig. 3, we visualize the approximation for the effective bulk modulus inside the cavity. We choose shifted sigmoid functions as our basis functions because we assume the bulk modulus changes strongly when the mold is completely filled. This assumption can also be observed in [15], which presents estimates for a lumped parameter, closely related to the bulk modulus, obtained from a Kalman Filter implementation. During injection, we assume that the bulk modulus increases as residual air with a low bulk modulus is expelled from the cavity. The bulk modulus is also not expected to decrease during the material's solidification. Consequently, we enforce the bulk modulus to be a non-decreasing function by constraining the weights to be greater than zero ($w_i > 0$).

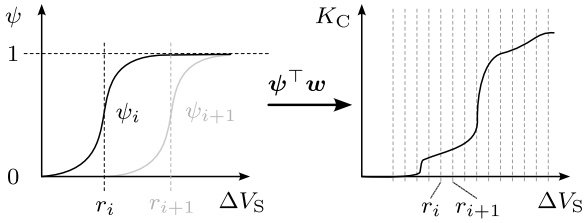

Fig. 3. Modeling approach for the bulk modulus K_C as a function of the displaced screw volume ΔV_S.

3.5. Modeling the volumetric flow rate

The volumetric flow rate entering the mold is approximated using the adapted power-law model

$$Q_\mathrm{C} = C_1 \cdot (p_\mathrm{S} - p_\mathrm{C})^{\frac{1}{C_2}} \cdot \exp\left(-C_3 \cdot t\right) \tag{8}$$

considering non-Newtonian and time-variant fluid behavior [1]. The lumped coefficient C_1 contains geometric and fluid-property information. We use the power-law-fluid coefficient $C_2 \neq 1$ to model the non-Newtonian fluid behavior. For simplicity, we assume that the viscosity follows an exponential trend over time influenced by the coefficient C_3. This exponential term is intended to approximate the influence of the solidification process on the viscosity of the melt.

3.6. System states and outputs

The state vector

$$\boldsymbol{x} = \begin{pmatrix} V_\mathrm{S} & Q_\mathrm{S} & p_\mathrm{S} & p_\mathrm{C} & t\end{pmatrix}^\top \in \mathbb{R}^{N_\boldsymbol{x}\times 1} \tag{9}$$

contains all $N_\boldsymbol{x} = 5$ system-state variables. We include the time variable t as an additional state variable, since (8) is time-variant. This transformation is a design choice intended to ease the formulation and implementation of the Optimal Control Problem (OCP) in Section 5. The model parameter vector

$$\boldsymbol{\Theta} = \begin{pmatrix} T_\mathrm{D} & K_\mathrm{D} & K_\mathrm{S} & \dot{S} & \boldsymbol{w}^\top & C_1 & C_3\end{pmatrix}^\top \in \mathbb{R}^{N_\boldsymbol{\Theta}\times 1} \tag{10}$$

contains the $N_\boldsymbol{\Theta}$ parameters optimized by the model optimizer. The parameters C_2 and V_C are set beforehand. Since the relationship between C_2 and Q_C is highly nonlinear and Q_C cannot be measured, we chose a reasonable value for the power-law index C_2 to simplify the model fitting. The geometric parameter V_C can be easily determined given the CAD model of the part and the runner. The resulting system of ordinary differential equations

$$\frac{\mathrm{d}\boldsymbol{x}}{\mathrm{d}t} = \boldsymbol{f}(\boldsymbol{x}, u_\mathrm{S}, \boldsymbol{\Theta}) = \begin{pmatrix}\dot{V}_\mathrm{S} & \dot{Q}_\mathrm{S} & \dot{p}_\mathrm{S} & \dot{p}_\mathrm{C} & 1\end{pmatrix}^\top \in \mathbb{R}^{N_\boldsymbol{x}\times 1} \tag{11}$$

and the equation for the $N_y = 4$ outputs

$$\boldsymbol{y} = \begin{pmatrix} V_S & Q_S & p_S & p_C \end{pmatrix}^\top \in \mathbb{R}^{N_y \times 1} \tag{12}$$

form a nonlinear time-variant state space model, whose model parameters are updated after each cycle using the model optimizer.

4. Model optimizer

4.1. Measurement preprocessing

In Fig. 4, we depict the routine executed inside the model optimizer in each time step. During the execution of the cavity-pressure controller, the optimizer saves the measurements of the state vector inside a buffer of length N_B for each state variable, overwriting existing observations from the previous cycle. After the controller finishes its task, the model optimizer approximates the time derivatives of the state vector $\boldsymbol{x}$ from (12) for each time step i using

$$\dot{\boldsymbol{x}}(i) \approx \begin{cases} \frac{4\boldsymbol{x}(2) - \boldsymbol{x}(3) - 3\boldsymbol{x}(1)}{2\Delta t} & \text{if} \quad i = 1 \\ \frac{\boldsymbol{x}(i+1) - \boldsymbol{x}(i-1)}{2\Delta t} & \text{if} \quad i \in [2, N_B - 1] \\ \frac{-4\boldsymbol{x}(N_B - 1) + \boldsymbol{x}(N_B - 2) + 3\boldsymbol{x}(N_B)}{2\Delta t} & \text{if} \quad i = N_B \end{cases} \tag{13}$$

as a second-order finite-difference stencil. We denote with $\boldsymbol{x}(i)$, the state vector for each time step i. Here, we cannot rely on the EKF estimates because there is no initial model parametrization. Between the cycles, the approximations of $\dot{\boldsymbol{x}}$ are used inside the model optimization loop.

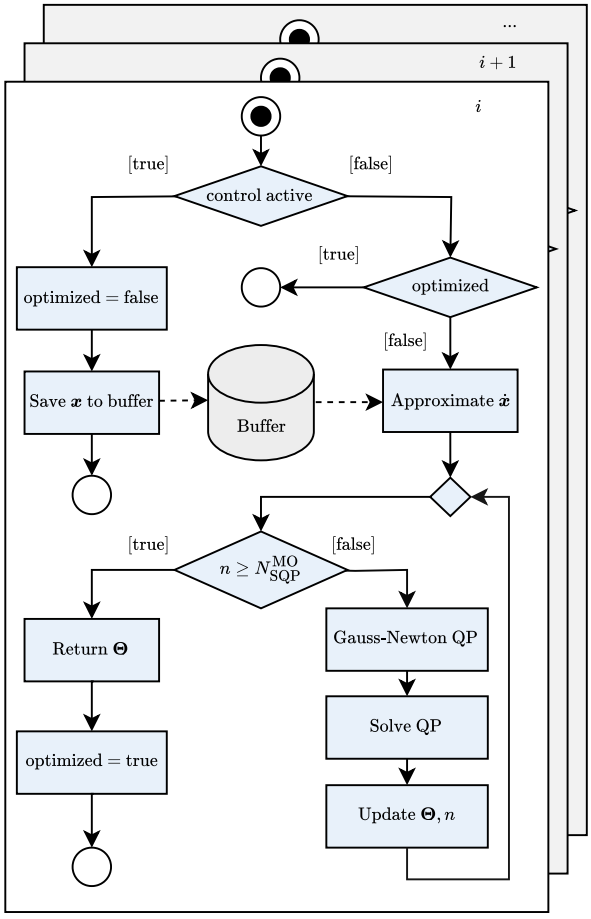

Fig. 4. Routine for model optimization that is executed at each time step i.

4.2. Parameter optimization

To parameterize the model, we use a sequential quadratic programming (SQP) approach to guide the optimization algorithm toward physically meaningful parameters by formulating appropriate constraints. Here, we enforce that all parameters in $\boldsymbol{\Theta}$ are positive. For the bulk modulus in combination with the sigmoid basis functions, this results in a non-decreasing function for K_C with its argument ΔV_S. We obtain $\boldsymbol{\Theta}^*$ as the optimizer of

$$\begin{aligned} \min_{\boldsymbol{\Theta}} \quad & \frac{1}{2} \boldsymbol{r}_{MO}(\boldsymbol{\Theta})^\top \boldsymbol{r}_{MO}(\boldsymbol{\Theta}) \\ \text{subject to} \quad & \underbrace{\boldsymbol{b}_{ieq}^{MO}(\boldsymbol{\Theta}) < \boldsymbol{0}}_{\text{Inequality constraints}} . \end{aligned} \tag{14}$$

Herein, $\boldsymbol{b}_{ieq}^{MO}$ contains the inequality constraints. The residual vector

$$\boldsymbol{r}_{MO}(\boldsymbol{\Theta}) = \dot{\boldsymbol{X}} - \boldsymbol{F} \tag{15}$$

contains the differences of all approximated temporal derivatives

$$\dot{\boldsymbol{X}} = \begin{pmatrix} \dot{\boldsymbol{x}}(1)^\top & \dots & \dot{\boldsymbol{x}}(N_B)^\top \end{pmatrix}^\top \in \mathbb{R}^{(N_{\boldsymbol{x}} \cdot N_B) \times 1} \tag{16}$$

from (13) and all temporal derivatives

$$\boldsymbol{F} = \begin{pmatrix} \boldsymbol{f}(\boldsymbol{x}(1), u_S(1), \boldsymbol{\Theta}) \\ \vdots \\ \boldsymbol{f}(\boldsymbol{x}(N_B), u_S(N_B), \boldsymbol{\Theta}) \end{pmatrix} \in \mathbb{R}^{(N_{\boldsymbol{x}} \cdot N_B) \times 1} \tag{17}$$

predicted by the model using (11). Since problem (14) is of nonlinear least-squares type, we employ a Gauss–Newton SQP approach to efficiently calculate the approximate Hessian $\mathbf{H}_{QP}^{MO}$ of the SQP [26]. The resulting quadratic sub-problem for the n-th SQP step can then be written as the quadratic program

$$\begin{aligned} \min_{\Delta\boldsymbol{\Theta}(n)} \quad & \frac{1}{2} \Delta\boldsymbol{\Theta}(n)^\top \mathbf{H}_{QP}^{MO}(n) \Delta\boldsymbol{\Theta}(n) \\ & + \boldsymbol{f}_{QP}^{MO}(n)^\top \Delta\boldsymbol{\Theta}(n) \\ \text{subject to} \quad & \mathbf{A}_{ieq}^{MO}(n)\, \Delta\boldsymbol{\Theta}(n) < -\boldsymbol{b}_{ieq}^{MO}(\boldsymbol{\Theta}(n)) \end{aligned} \tag{18}$$

with

$$\mathbf{H}_{QP}^{MO}(n) = \left(\frac{\partial \boldsymbol{r}_{MO}}{\partial \boldsymbol{\Theta}} \Big|_{\boldsymbol{\Theta}(n)} \right)^\top \left(\frac{\partial \boldsymbol{r}_{MO}}{\partial \boldsymbol{\Theta}} \Big|_{\boldsymbol{\Theta}(n)} \right) \in \mathbb{R}^{N_{\boldsymbol{\Theta}} \times N_{\boldsymbol{\Theta}}}, \tag{19}$$

$$\boldsymbol{f}_{QP}^{MO}(n) = \left(\frac{\partial \boldsymbol{r}_{MO}}{\partial \boldsymbol{\Theta}} \Big|_{\boldsymbol{\Theta}(n)} \right)^\top \boldsymbol{r}_{MO}(\boldsymbol{\Theta}(n)) \in \mathbb{R}^{N_{\boldsymbol{\Theta}} \times 1}, \tag{20}$$

$$\mathbf{A}_{ieq}^{MO}(n) = \left(\frac{\partial \boldsymbol{b}_{ieq}^{MO}}{\partial \boldsymbol{\Theta}} \Big|_{\boldsymbol{\Theta}(n)} \right) \in \mathbb{R}^{N_\psi \times N_{\boldsymbol{\Theta}}}, \tag{21}$$

evaluated at the current iterate $\boldsymbol{\Theta}(n)$ of the parameter vector. The matrix $\mathbf{H}_{QP}^{MO}$ is the approximated Hessian matrix. The vector $\boldsymbol{f}_{QP}^{MO}$ denotes the gradient vector. The linear inequality matrix is $\mathbf{A}_{ieq}^{MO}$. Here, we denote the deviation from the current parameter-vector iterate with $\Delta\boldsymbol{\Theta}$. In accordance with Fig. 4, we repeat solving (18) for N_{SQP}^{MO} times while updating $\boldsymbol{\Theta}$ according to

$$\boldsymbol{\Theta}(n+1) = \boldsymbol{\Theta}(n) + \alpha_{SQP} \Delta\boldsymbol{\Theta}(n) \tag{22}$$

with the factor $\alpha_{SQP} \in \,]\,0,\,1[$ to damp the SQP step. The optimized model is then used within the NMPC and the EKF for the next cycle.

5. NMPC and EKF

5.1. Optimal control problem

To formulate the OCP, we first need to define

$$\boldsymbol{X} = \begin{pmatrix} \boldsymbol{x}(1)^\top & \cdots & \boldsymbol{x}(N_1)^\top \end{pmatrix}^\top \in \mathbb{R}^{(N_{\boldsymbol{x}} \cdot N_1) \times 1} \tag{23}$$

to consist of all states within the prediction horizon of length N_1. Consequently,

$$\boldsymbol{p}_C = \begin{pmatrix} p_C(1) & \cdots & p_C(N_1) \end{pmatrix} \in \mathbb{R}^{N_1 \times 1} \tag{24}$$

contains the cavity-pressure entries, and

$$\boldsymbol{p}_{\mathrm{C}}^{\mathrm{ref}} = \begin{pmatrix} p_{\mathrm{C}}^{\mathrm{ref}}(1) & \cdots & p_{\mathrm{C}}^{\mathrm{ref}}(N_1) \end{pmatrix} \in \mathbb{R}^{N_1 \times 1} \tag{25}$$

contains the cavity-pressure reference for each point inside the prediction horizon. The vector

$$\boldsymbol{U} = \begin{pmatrix} u_{\mathrm{S}}(1) & \dots & u_{\mathrm{S}}(N_2) \end{pmatrix}^{\top} \in \mathbb{R}^{N_2 \times 1} \tag{26}$$

contains the input variables u_{S} for each time step within the control horizon of length N_2. The uncondensed vector of optimization variables

$$\boldsymbol{\xi} = \begin{pmatrix} \boldsymbol{X}^{\top} & \boldsymbol{U}^{\top} & \eta \end{pmatrix}^{\top} \in \mathbb{R}^{N_\xi} \tag{27}$$

contains the state variables $\boldsymbol{X}$, the inputs $\boldsymbol{U}$, and a slack variable η. Consequently, the number of uncondensed optimization variables is

$$N_\xi = N_{\boldsymbol{x}} \cdot N_1 + N_2 + 1 \ . \tag{28}$$

The optimal control problem (OCP)

$$\begin{aligned} \min_{\boldsymbol{\xi}} \quad & \underbrace{\frac{1}{2}(\boldsymbol{p}_{\mathrm{C}} - \boldsymbol{p}_{\mathrm{C}}^{\mathrm{ref}})^{\top} Q (\boldsymbol{p}_{\mathrm{C}} - \boldsymbol{p}_{\mathrm{C}}^{\mathrm{ref}})}_{\text{Tracking penalty}} + \underbrace{\frac{1}{2}\delta\boldsymbol{U}^{\top} R \delta\boldsymbol{U}}_{\text{Actuator penalty}} \\ & + \underbrace{\frac{1}{2}\,\rho\,\eta^2}_{\text{Overshoot penalty}} \\ \text{subject to} \quad & \underbrace{\boldsymbol{b}_{\mathrm{eq}}^{\mathrm{MPC}} = \boldsymbol{0}}_{\text{Equality constraints}} \quad \text{and} \\ & \underbrace{\boldsymbol{b}_{\mathrm{ieq}}^{\mathrm{MPC}} < \boldsymbol{0}}_{\text{Inequality constraints}} \ , \end{aligned} \tag{29}$$

consists of a penalty for deviating from the cavity-pressure reference $\boldsymbol{p}_{\mathrm{C}}^{\mathrm{ref}}$ weighted by $Q \in \mathbb{R}^{+}$. Additionally, the cost function of the OCP includes an actuator penalty that penalizes the time-discrete temporal derivative

$$\delta\boldsymbol{U} = \begin{pmatrix} u_{\mathrm{S}}(1) - u_{\mathrm{S}}(0) \\ \vdots \\ u_{\mathrm{S}}(N_2) - u_{\mathrm{S}}(N_2 - 1) \end{pmatrix} \in \mathbb{R}^{N_2 \times 1} \tag{30}$$

of the control input within the control horizon weighted by $R \in \mathbb{R}^{+}$. Overshoots over the desired cavity-pressure reference are weighted using the factor $\rho \in \mathbb{R}^{+}$, utilizing the slack variable $\eta \in \mathbb{R}^{+}$ to soften up the maximum cavity-pressure constraint.

The equality constraints

$$\underbrace{\begin{pmatrix} \boldsymbol{x}(1) - \mathrm{RK4}(\boldsymbol{f}(\hat{\boldsymbol{x}}, u_{\mathrm{S}}(0)), \Delta t) \\ \boldsymbol{x}(2) - \mathrm{RK4}(\boldsymbol{f}(\boldsymbol{x}(1), u_{\mathrm{S}}(1)), T_{\mathrm{int}}) \\ \vdots \\ \boldsymbol{x}(i+1) - \mathrm{RK4}(\boldsymbol{f}(\boldsymbol{x}(i), u_{\mathrm{S}}(\min(i, N_2)), T_{\mathrm{int}}) \end{pmatrix}}_{\boldsymbol{b}_{\mathrm{eq}}^{\mathrm{MPC}} \in \mathbb{R}^{(N_{\boldsymbol{x}} \cdot N_1) \times 1}} = \boldsymbol{0} \tag{31}$$

correspond to the nonlinear system dynamics integrated using an explicit Runge–Kutta 4th order scheme (RK4) using the integration time-step size T_{int}. Here, i denotes the time step inside the prediction horizon. We use the min function in (31), because the control horizon is smaller than the prediction horizon. Thus, holding the last controller output over the remaining part of the prediction horizon is a natural choice. Note here that $\boldsymbol{x}(1)$ is not equal to the estimated state of the EKF. Since the controller output is applied to the plant at the end of each time step, the effect of the last controller output $u_{\mathrm{S}}(0)$ must be predicted with the estimated state $\hat{\boldsymbol{x}}$ from the EKF and the time-step size Δt.

We consider inequality constraints

$$\underbrace{\begin{pmatrix} \boldsymbol{U} - \boldsymbol{1}^{N_2 \times 1} u_{\mathrm{S,lim}}^{+} \\ (-1)\boldsymbol{U} + \boldsymbol{1}^{N_2 \times 1} u_{\mathrm{S,lim}}^{-} \\ \boldsymbol{p}_{\mathrm{C}} - \boldsymbol{p}_{\mathrm{C,lim}} - \boldsymbol{1}^{N_1 \times 1}\eta \\ -\eta \end{pmatrix}}_{\boldsymbol{b}_{\mathrm{ieq}}^{\mathrm{MPC}} \in \mathbb{R}^{(2 \cdot N_2 + N_1 + 1) \times 1}} < \boldsymbol{0}, \tag{32}$$

in the form of upper bounds $u_{\mathrm{S,lim}}^{+}$ and lower bounds $u_{\mathrm{S,lim}}^{-}$ for the inputs, which serve as a simple way to limit the velocity of the screw. Furthermore, we consider a maximum pressure constraint $\boldsymbol{p}_{\mathrm{C,lim}}$ for the cavity pressure to prevent overshoots. Here, we use the slack variable η to soften up the constraint. We denote with $\boldsymbol{1}$ the identity vector with the dimension information given inside the superscript. We define $\boldsymbol{p}_{\mathrm{C,lim}}$ as

$$\boldsymbol{p}_{\mathrm{C,lim}} = \boldsymbol{p}_{\mathrm{C}}^{\mathrm{ref}} + \boldsymbol{1}^{N_1 \times 1} \Delta p_{\mathrm{C,OS}} \tag{33}$$

with respect to the cavity-pressure reference vector $\boldsymbol{p}_{\mathrm{C}}^{\mathrm{ref}}$ and the maximum allowed cavity-pressure overshoot denoted with $\Delta p_{\mathrm{C,OS}} \in \mathbb{R}$.

5.2. Sequential quadratic programming

Since the OCP is a constrained nonlinear least-squares problem, we again employ a Gauss–Newton SQP approach to solve this OCP. The residual vector

$$\boldsymbol{r}_{\mathrm{MPC}} = \begin{pmatrix} \sqrt{Q}(\boldsymbol{p}_{\mathrm{C}} - \boldsymbol{p}_{\mathrm{C}}^{\mathrm{ref}}) \\ \sqrt{R}\delta\boldsymbol{U} \\ \sqrt{\rho}\eta \end{pmatrix} \in \mathbb{R}^{N_\xi \times 1} \tag{34}$$

can be directly determined from the OCP in (29). The quadratic program for the SQP iteration n then takes the form

$$\begin{aligned} \min_{\Delta\boldsymbol{\xi}(n)} \quad & \frac{1}{2}\Delta\boldsymbol{\xi}(n)^{\top}\mathbf{H}_{\mathrm{QP}}^{\mathrm{MPC}}(n)\Delta\boldsymbol{\xi}(n) + \boldsymbol{f}_{\mathrm{QP}}^{\mathrm{MPC}}(n)^{\top}\Delta\boldsymbol{\xi}(n) \\ \text{subject to} \quad & \mathbf{A}_{\mathrm{eq}}^{\mathrm{MPC}}(n)\Delta\boldsymbol{\xi}(n) = (-1)\boldsymbol{b}_{\mathrm{eq}}^{\mathrm{MPC}}(\boldsymbol{\xi}(n)) \\ & \mathbf{A}_{\mathrm{ieq}}^{\mathrm{MPC}}(n)\Delta\boldsymbol{\xi}(n) < (-1)\boldsymbol{b}_{\mathrm{ieq}}^{\mathrm{MPC}}(\boldsymbol{\xi}(n)) \end{aligned} \tag{35}$$

with the approximation of the uncondensed Hessian matrix

$$\mathbf{H}_{\mathrm{QP}}^{\mathrm{MPC}}(n) = \left(\frac{\partial \boldsymbol{r}_{\mathrm{MPC}}}{\partial \boldsymbol{\xi}}\bigg|_{\boldsymbol{\xi}(n)} \right)^{\top} \frac{\partial \boldsymbol{r}_{\mathrm{MPC}}}{\partial \boldsymbol{\xi}}\bigg|_{\boldsymbol{\xi}(n)} \in \mathbb{R}^{N_\xi \times N_\xi}, \tag{36}$$

the uncondensed gradient vector

$$\boldsymbol{f}_{\mathrm{QP}}^{\mathrm{MPC}}(n) = \left(\frac{\partial \boldsymbol{r}_{\mathrm{MPC}}}{\partial \boldsymbol{\xi}}\bigg|_{\boldsymbol{\xi}(n)} \right)^{\top} \boldsymbol{r}_{\mathrm{MPC}}(\boldsymbol{\xi}(n)) \in \mathbb{R}^{N_\xi \times 1}, \tag{37}$$

the uncondensed Jacobians

$$\mathbf{A}_{\mathrm{eq}}^{\mathrm{MPC}}(n) = \frac{\partial \boldsymbol{b}_{\mathrm{eq}}^{\mathrm{MPC}}}{\partial \boldsymbol{\xi}}\bigg|_{\boldsymbol{\xi}(n)} \in \mathbb{R}^{(N_{\boldsymbol{x}} \cdot N_1) \times N_\xi}, \tag{38}$$

$$\mathbf{A}_{\mathrm{ieq}}^{\mathrm{MPC}}(n) = \frac{\partial \boldsymbol{b}_{\mathrm{ieq}}^{\mathrm{MPC}}}{\partial \boldsymbol{\xi}}\bigg|_{\boldsymbol{\xi}(n)} \in \mathbb{R}^{(2 \cdot N_2 + N_1 + 1) \times N_\xi}, \tag{39}$$

of the constraints with respect to the optimization variables, and the deviation from the last iterate of the uncondensed vector of optimization variables

$$\Delta\boldsymbol{\xi} = \begin{pmatrix} \Delta\boldsymbol{X}^{\top} & \Delta\boldsymbol{U}^{\top} & \Delta\eta \end{pmatrix}^{\top} \in \mathbb{R}^{N_\xi \times 1}. \tag{40}$$

During the SQP algorithm, we update the new vector of the optimization variables using

$$\boldsymbol{\xi}(n+1) = \boldsymbol{\xi}(n) + \alpha_{\mathrm{SQP}}\Delta\boldsymbol{\xi}(n). \tag{41}$$

The parameter $\alpha_{\mathrm{SQP}} \in \ ]\,0,\ 1[$ is chosen to damp the SQP step. The presented algorithm is repeated $N_{\mathrm{SQP}}^{\mathrm{MPC}}$ times before applying $u_{\mathrm{S}}(1)$ to the plant at the end of the time step. To bound the computational effort, we employ a standard 'suboptimal MPC' strategy by using a fixed number of SQP iterations $N_{\mathrm{SQP}}^{\mathrm{MPC}}$. The disadvantage of this practical approach is that the optimal solution might not be found within the admissible number of SQP iterations.

5.3. Condensing of the OCP

Since the resulting QP is of high dimension and we employ a QP solver for dense Hessians, we reduce the dimension of the OCP by applying a condensing algorithm. The condensing approach rearranges the linearized equality constraints and replaces the dependent variables $\Delta \boldsymbol{X}$ in the original OCP. Following this approach, the number of optimization variables can be reduced from $N_\xi = N_{\boldsymbol{x}} \cdot N_1 + N_2 + 1$ to $N_2 + 1$, obtaining a dense version of the Hessian matrix [27]. In this case, adding the time t as an additional model state in Section 3 does not affect the QP size.

In Fig. 5, we visualize the algorithm that runs in each time step when the cavity-pressure controller is active.

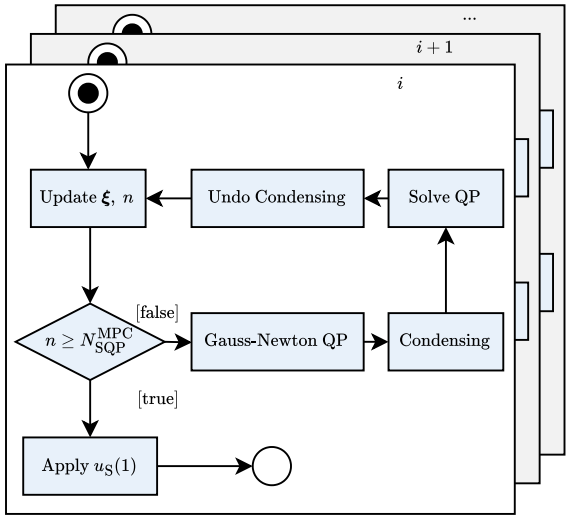

Fig. 5. Routine for the model predictive cavity-pressure controller executed at each time step i.

5.4. Rediscretization of the OCP

To further reduce computational complexity, we rediscretize the OCP using the new prediction sample time T_{int}. Within the prediction horizon, we multiply the time step size Δt by factor $\kappa \in \mathbb{N}^+$:

$$T_{\text{int}} = \kappa \cdot \Delta t \ . \tag{42}$$

This approach artificially increases the length of the prediction horizon by a factor of κ without increasing the computational complexity of the calculations. However, it introduces numerical errors due to the broader discretization. After each Δt, the NMPC loop is repeated.

5.5. Extended Kalman filter

The EKF implementation also uses the model described in Section 3. The EKF can be used to denoise the measurement signal or to estimate unmeasurable states. In MPC, a common approach is to integrate an error state to enable offset-free tracking. In our work, we decided against using an error-state EKF because the implementation in injection molding is not straightforward. Applying an error-state estimator naively can lead to extremely large error states when the event of cavity filling is mispredicted. The measurement noise covariance matrix is chosen to be the diagonal matrix

$$\mathbf{R}_{\text{EKF}} = \text{diag}(\sigma^2_{V_{\text{S}}}, \sigma^2_{Q_{\text{S}}}, \sigma^2_{p_{\text{S}}}, \sigma^2_{p_{\text{C}}}) \in \mathbb{R}^{N_{\boldsymbol{y}} \times N_{\boldsymbol{y}}} \tag{43}$$

where the diagonal elements represent the variances of the individual measured outputs, as indicated by their respective subscripts. These values were identified during the standstill phase of the injection molding machine and are summarized in Table 2. The process noise covariance matrix is chosen to be

$$\mathbf{Q}_{\text{EKF}} = \begin{pmatrix} q_{\text{EKF}} \mathbf{R}_{\text{EKF}} & \mathbf{0}^{N_{\boldsymbol{y}} \times 1} \\ \mathbf{0}^{1 \times N_{\boldsymbol{y}}} & 0^{1 \times 1} \end{pmatrix} \in \mathbb{R}^{N_{\boldsymbol{x}} \times N_{\boldsymbol{x}}}, \tag{44}$$

with a tuning parameter $q_{\text{EKF}} \in \mathbb{R}^+$. In our work, we adopt a high process variance by setting q_{EKF} to a large value. By choosing a large value, we place greater trust in the measurements, since the model is learned during manufacturing and the quality of its predictions is unknown. An additional zero entry is added for the time variable, because the differential equation used to predict the time is exact.

6. Control of part mass

6.1. Gaussian process regression model

We use a Gaussian process regression (GPR) model [28,29] with a linear prior function to model the relationship between the cavity-pressure reference $p_{\text{C}}^{\text{ref}}$ and the resulting part mass m. We adopt a data-driven modeling approach because it avoids modeling complex physical phenomena, such as the influence of the non-return valve's closing dynamics on the part mass. Furthermore, it eliminates reliance on detailed material models, which are typically unavailable due to batch-to-batch fluctuations during PCR processing. The Gaussian process of the predicted mass

$$\hat{m} \sim \mathcal{GP}\left(\phi(p_{\text{C}}^{\text{ref}}), k\right) \tag{45}$$

is defined by the linear mean function ϕ and the kernel function k.

6.2. Cycle-variant kernel function

In industrial practice new material is fed to the hopper. Therefore, we assume the transition between material batches spans multiple cycles, as different batches blend within the hopper and during dosing. Consequently, as material properties change, recent observations hold greater value than past observations. To account for this idea, we use the kernel extension presented in [30]. The resulting kernel function

$$k = k_{\text{SE}}(p_{\text{C}}^{\text{ref}}, p_{\text{C}}^{\text{ref}\prime}) \cdot k_{\text{W}}(c, c') \tag{46}$$

is a product of the squared-exponential kernel function

$$k_{\text{SE}}(p_{\text{C}}^{\text{ref}}, p_{\text{C}}^{\text{ref}\prime}) = \sigma_0^2 \exp\left(-\frac{\|p_{\text{C}}^{\text{ref}} - p_{\text{C}}^{\text{ref}\prime}\|_2^2}{2l^2}\right) \tag{47}$$

and a Wiener kernel

$$k_{\text{W}}(c, c') = {\sigma_{\text{W}}}^2(\min(c, c') - C_0), \tag{48}$$

as a function of the cycle number c and the parameter $C_0 = -{\sigma_{\text{W}}}^{-2}$ [30]. The variance hyperparameter σ_0 controls the scale of the kernel function. The hyperparameter l determines the characteristic length over which the function varies. It describes how much a pair of features $p_{\text{C}}^{\text{ref}}$ and $p_{\text{C}}^{\text{ref}\prime}$ covary with each other. The parameter σ_{W} is the variance hyperparameter of the Wiener kernel. Maximizing the marginal log-likelihood function yields the hyperparameters

$$\boldsymbol{\Theta}_{\text{GPR}} = \begin{pmatrix} \sigma_0 & \sigma_{\text{W}} & l & \sigma \end{pmatrix}^\top \tag{49}$$

after each model update. We use Matlab's internal Gaussian process regression toolbox (*fitrgp*) with the kernel function introduced in (46) [31].

6.3. Obtaining the next reference for cavity pressure

Obtaining a new cavity-pressure reference p_C^{ref} is carried out by minimizing the square of the Euclidean distance between the expectation value of the Gaussian process $\mathbb{E}(\hat{m})$ and the desired mass m^{ref}. For the optimization, we define lower and upper limits for the optimization variable p_C^{ref}. To prevent damage to the mold or IM machine, we impose upper limits on the cavity-pressure reference. The lower limit is set by the reference pressure required to completely fill the part. Since the underlying surrogate model for the mass is updated between cycles, and we process different batches of material, preventing the algorithm from demanding dangerous cavity-pressure references is crucial. As a result, the desired mass may not be attainable when transitioning between materials, because the required cavity-pressure reference may lie outside the admissible range. The optimizer

$$p_C^{ref,*} = \underset{p_C^{ref}}{\operatorname{argmin}} \quad \left(\mathbb{E}(\hat{m}) - m^{ref}\right)^2$$
$$\text{subject to} \quad p_C^{ref,min} \le p_C^{ref} \le p_C^{ref,max}$$

is used as a constant cavity-pressure reference for the next cycle.

Fig. 6 illustrates the routine executed during each IM cycle to control the part mass. During the initial experiments with a new material or mold, no part mass model is available. Therefore, p_C^{ref} is selected from a predefined set of c_{ident} initial cavity-pressure references. Once these initial cycles are complete, a new cavity-pressure reference is optimized to achieve the desired part mass m^{ref}. As new part mass measurements become available in subsequent cycles, the underlying GP model is continuously updated.

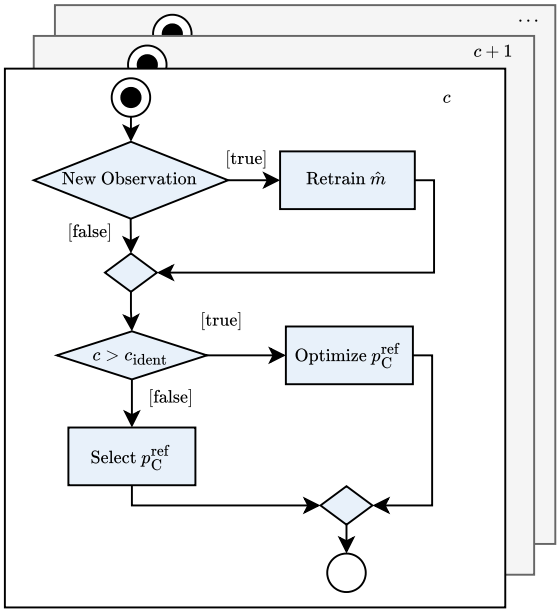

Fig. 6. Routine for the part-mass controller for different cycles c.

7. Experimental setup

7.1. Injection molding hardware

We tested the developed control approach from Fig. 1 on the servo-electric injection molding machine Allrounder 520 A 1500-800, supplied by Arburg GmbH & Co. KG (Loßburg, Germany). We used a screw with a diameter of 35 mm.

The external real-time control hardware PXI-8108 and the NI PXI-7842R FPGA module, manufactured by National Instruments (Austin, USA), are used to control the injection molding machine.

In this publication, we conducted experiments using the plate geometry depicted in Fig. 7. The mold geometry is representative of thin-walled parts in industrial practice, making it an appropriate choice for the following evaluations.

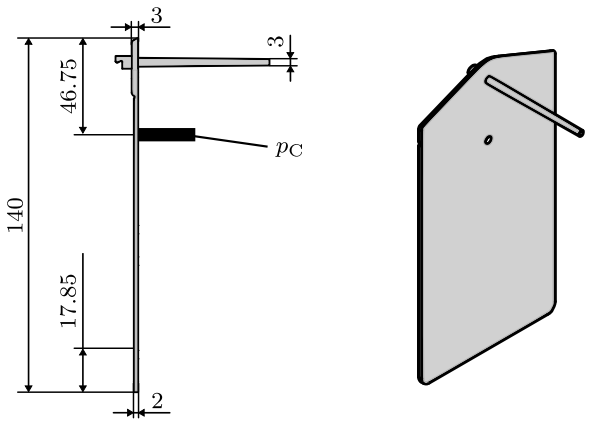

Fig. 7. The plate part used to test the control approach, adapted from [16]. The part dimensions are given in mm.

7.2. Processed materials

We used a polypropylene PP579S supplied by Sabic Deutschland GmbH &Co. KG (Düsseldorf, Germany) as the virgin material. Additionally, Systec GmbH (Cologne, Germany) supplied five batches of PCR polypropylene material (Systalen PP-24000 gr000). In the prior publication [32], the authors investigated the melt flow rate according to DIN EN ISO 1133. The polymer densities were determined experimentally according to DIN EN ISO 11744. Both the MFR and polymer density are shown in Table 1. The MFR material exhibited variations of 20 % in both melt flow rate and polymer density. The MFR values differ between the virgin and selected PCR materials. This selection of materials allows us to test our control approach with the worst-case scenario of a material transition, such as between batches from different manufacturers. To investigate the effect of the PCR material on the proposed control approach, we selected batches A, C, and E. Since the MFR values of the remaining batches fall within the range of those used for testing, they offer limited additional benefit. The part mass was measured using a laboratory scale produced by Kern & Sohn GmbH (Balingen, Germany).

Table 1
Melt flow rate (MFR) and density for virgin and PCR material, adapted from [32]. The MFR was measured at a temperature of 230 °C using a test weight of 2.16 kg.

Material	Batch	MFR g/(10 min)	Density g/cm³
Virgin		47.00	0.905
PCR	A	13.90	0.947
	C	11.64	0.950
	E	10.31	0.952

7.3. Injection molding software

We implemented the previously mentioned algorithms in MATLAB and Simulink using the CasADi framework [33]. Matlab and Simulink were developed by Mathworks (Natick, USA) [31].

At the beginning of each injection phase of the cycle, the injection molding machine is actuated in a feedforward manner with the maximum screw velocity caused by the controller signal $u_{S,lim}^{-}$ until the activation pressure of $p_C = 5$ bar is reached. This ensures a smooth transition between the feedforward machine-internal controller and our developed cavity-pressure controller. Since the P controller does not predict the event of complete cavity filling, it is allowed to retract the

screw. Once the activation pressure is reached, the proposed process controller is engaged and operates for a predefined duration of $T_C = 5\,s$. The rather short cycle time is due to the thin-walled geometry under investigation. After this period t_C, our controller is deactivated, and the machine's internal control system takes over to manage the cooling phase and prepare for the next cycle. Fig. 8 illustrates the cavity-pressure control sequence over a single production cycle. Effectively, the active period of the process controller corresponds to the injection and packing phases of the conventional control strategy for IM.

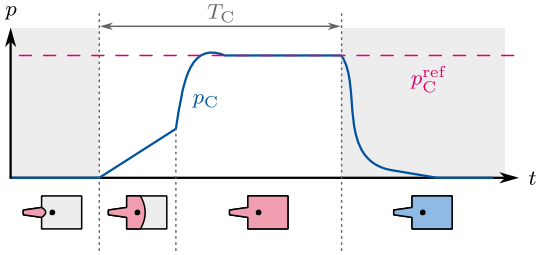

Fig. 8. Proposed cavity-pressure-control sequence. The process controller is active during the period t_C.

7.4. Batch transitions

To closely follow industrial practice, we added material directly to the hopper of the injection molding machine, allowing for a mixture of two material batches. The transition from virgin material to PCR can be visually observed because the virgin material is transparent, while the PCR batches are gray. When transitioning between two PCR batches, we added coloring additives to one of the batches. The experimental data can be found in [34].

7.5. Experimental protocol

This publication presents four main experiments.

1. To evaluate the transition from P control to the learning-enabled NMPC, we ran four cycles using virgin and PCR materials and cavity-pressure references of 200 bar and 300 bar, respectively.

The following evaluations were initiated after the process model was successfully learned from a P-controlled cycle and four cycles were run using the NMPC controller.

2. To assess the closed-loop control performance for transitions between batches, we first switched from virgin material to PCR batch E at a reference cavity pressure of 200 bar. For a second evaluation, we added material from PCR batch C, switched back to virgin material, and ran three cycles at a reference cavity pressure of 300 bar.
3. To evaluate the closed-loop tracking behavior, we ran three cycles with virgin material at a reference cavity pressure of 200 bar. Then, we switched to a reference cavity pressure of 300 bar.
4. To evaluate the performance of the part-mass controller, we ran $c_{init} = 6$ initialization cycles at reference cavity-pressure values of 200 bar and 300 bar. We activated the part-mass controller at cycle 7. PCR batch E was visually detected in cycle 20. Then, we detected PCR batch A in cycle 42. We ended the experiment after 50 cycles.

All experiments were performed using the controller parameters according to Table 2.

Table 2
Parameters used for the experimental tests shown in Section 8.

Parameter name (See Sec.)	Value	Unit
V_C (3)	33.5	cm^3
C_2 (3)	0.5	–
N_ψ (3)	30	–
N_{SQP}^{MO} (4)	50	–
α_{SQP} (4)	0.7	–
N_1 (5)	15	–
N_2 (5)	4	–
ρ (5)	100	bar^{-2}
Q (5)	1	bar^{-2}
R (5)	$8 \cdot 10^4$	V^{-2}
$u_{S,lim}^{+}$ (5)	0	V
$u_{S,lim}^{-}$ (5)	−1	V
$\Delta p_{C,OS}$ (5)	5	bar
κ (5)	3	–
N_{SQP}^{MPC} (5)	2	–
α_{SQP} (5)	0.7	–
σ_{V_s} (5)	0.0128	cm^3
σ_{Q_s} (5)	0.0139	$cm^3 s^{-1}$
σ_{p_s} (5)	0.2020	bar
σ_{p_c} (5)	0.2231	bar
q_{EKF} (5)	100	–
σ_W (6)	15	–
$p_C^{ref,min}$ (6)	150	bar
$p_C^{ref,max}$ (6)	350	bar
K_P (7)	$8 \cdot 10^{-3}$	$V\,bar^{-1}$
Δt (7)	$8 \cdot 10^{-3}$	s
t_1 (7)	3	s
T_C (7)	5	s

7.6. Error metrics for process control

We use the root mean square error (RMSE) to assess the closed-loop tracking performance,

$$\mathrm{RMSE} = \sqrt{\frac{1}{N}\sum_{i=1}^{N}\left(p_C^{ref}(i) - p_C(i)\right)^2}. \tag{50}$$

Additionally, we evaluate the maximum cavity-pressure overshoot and the mean cavity-pressure offset.

The maximum cavity-pressure overshoot (OS)

$$\mathrm{OS} = \max(\boldsymbol{p}_C - \boldsymbol{p}_C^{ref}) \tag{51}$$

is vital for cavity-pressure control, since cavity-pressure peaks can damage the mold and result in part-surface defects [1].

The mean cavity-pressure offset (OF)

$$\mathrm{OF} = \frac{1}{N - \frac{t_1}{\Delta t}} \sum_{i=\frac{t_1}{\Delta t}}^{N} \left| p_C(i) - p_C^{ref}(i) \right|, \tag{52}$$

starting at $t = t_1$, is also a crucial parameter for our process-control approach. Because the outer control loop cannot consider differences between the cavity-pressure reference and controlled cavity pressure, these differences might cause increased uncertainty in the part-mass model.

8. Results

8.1. Initializing the NMPC with experimental data from a P controller

In Fig. 9, we present the cavity-pressure curves p_C with the volumetric flow rates Q_S induced by the screw velocity when starting

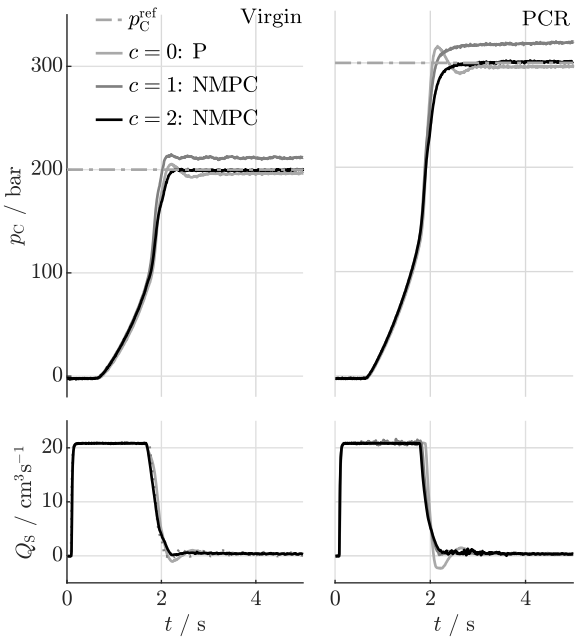

Fig. 9. Experimental results of closed-loop controller performance upon switching from the P controller to the learning-enabled NMPC using virgin material at 200 bar and using PCR batch C at 300 bar cavity-pressure reference.

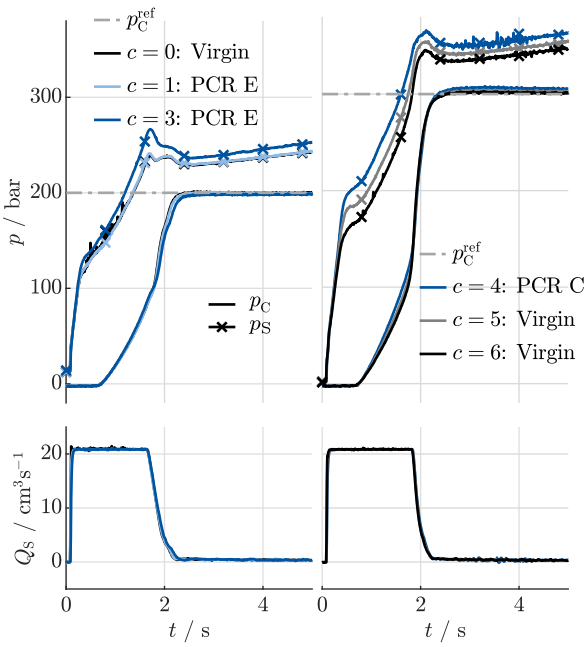

Fig. 10. Experimental cavity pressure p_C, screw pressure p_S, and volumetric flow rate Q_S for closed-loop NMPC under material change between batches.

up the algorithm. The Figure is divided between virgin material (left part of Fig. 9) and PCR batch C (right side of Fig. 9). These initial cycles are shown for cavity-pressure references of 200 bar and 300 bar. The experiments are presented in chronological order, from $c = 0$ to $c = 2$. For the experiments, the first cycle ($c = 0$) is obtained by utilizing the P controller that does not require a model of the underlying process. After the first run of the model optimizer, we switch to the NMPC (1: NMPC). The first generation of the learning-enabled NMPC (1: NMPC) overshoots the cavity-pressure reference for both pressure levels in Fig. 9 and shows a stationary offset between the reference and the measured cavity pressure, together with oscillations in the cavity pressure, primarily present in the left part of Fig. 9. Compared to the first generation of the NMPC, the second generation (2: NMPC) shows a reduced overshoot and offset between the cavity pressure and its reference. There are also no visible oscillations in the cavity pressure. The NMPC decreases Q_S earlier than the P controller.

8.2. Transitioning from virgin material to PCR

In Fig. 10, the behavior of the learning-enabled model predictive controller is presented when transitioning from virgin material to PCR batch E (left side of Fig. 10) and transitioning from PCR batch C back to the virgin material (right side of Fig. 10).

In addition to the cavity pressure p_C and the volumetric flow rate Q_S induced by the screw velocity, we also show the pressure p_S measured inside the screw antechamber. The screw pressure increases when transitioning from virgin material to PCR material and vice versa when returning to the virgin material. Additionally, slight deviations in the cavity pressure are visible, particularly on the right side of Fig. 10. The slope of the cavity pressure differs in the right half of Fig. 10. The slope for PCR is greater than that for virgin material.

In Fig. 11, the identified bulk moduli from (5) within the cavity are shown over the displaced volume of the screw ΔV_S for two different cycles. The solid line in Fig. 3 shows the bulk modulus of cycle $c = 14$. This cycle is carried out several cycles before the influence of the PCR material becomes apparent, thereby reflecting the bulk modulus of the virgin material. The dashed line represents the identified bulk modulus within the cavity, multiple cycles after we observe the effects of the PCR material. Therefore, the dashed line shows the bulk modulus of the PCR material. Both curves in Fig. 11 have a similar shape, but differ in height and show an offset in the direction of the displaced volume ΔV_S.

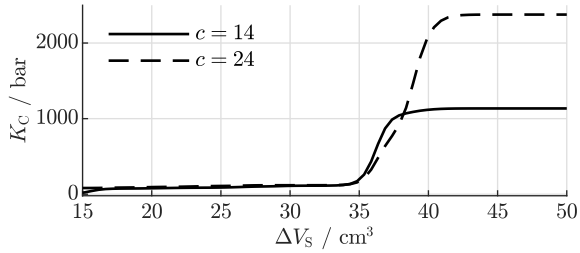

Fig. 11. Identified bulk moduli when switching from virgin material ($c = 14$) to PCR batch E ($c = 24$) as a function of the displaced screw volume ΔV_S.

8.3. Switching the cavity-pressure reference

In Fig. 12(a), the behavior of the learning-enabled NMPC is shown when transitioning from a cavity-pressure reference of 200 bar to 300 bar using the virgin material.

In Fig. 12(b), we visualize the performance metrics introduced in Section 7.6. When transitioning from a 200 bar to a 300 bar cavity-pressure reference, the RMSE initially increases but decreases over the following two controller generations. Fig. 12(a) shows a reduction in rise time for the 300 bar cavity-pressure curves (cycles 4 to 6) as the number of controller generations increases. Both the OS and the OF between the reference and the actual cavity pressure increase with the higher pressure reference.

8.4. Part-mass control by adapting the cavity-pressure reference

We use six experiments with two different initial pressure levels to initialize the part-mass prediction model of the controller. During part-mass control, we transition between three different materials. Starting with virgin material, we switch to PCR batch E at approximately cycle 22 and to PCR batch A at approximately cycle 42. The points of

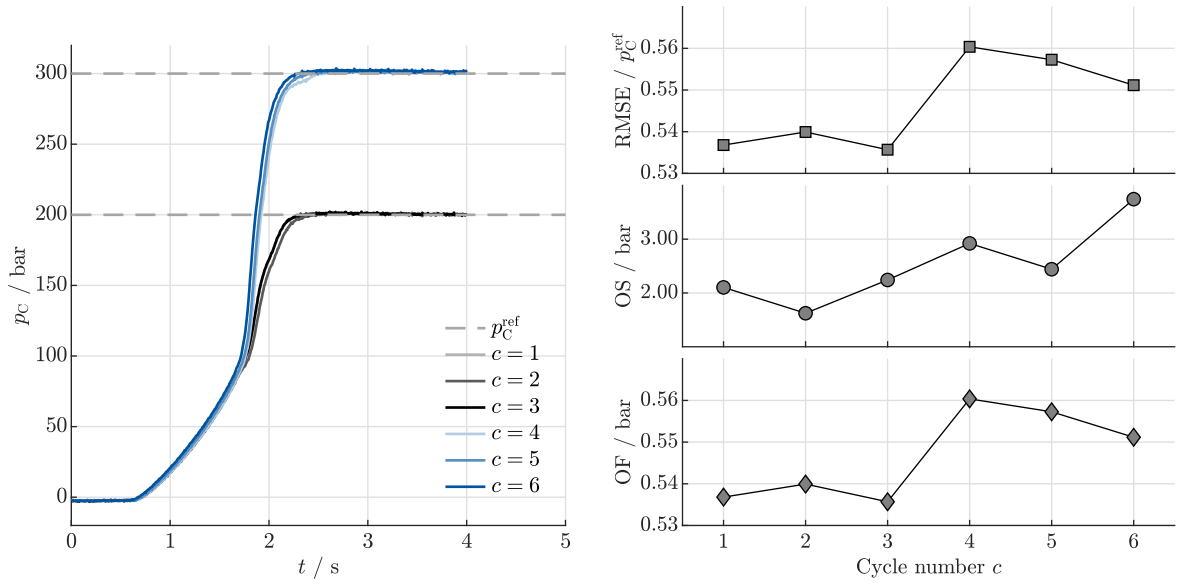

(a) Experimental cavity pressure p_C for tracking behavior of the NMPC when switching from 200 bar to 300 bar cavity-pressure reference processing virgin material.

(b) Root mean square error RMSE (50), maximum cavity-pressure overshoot OS (51) and static cavity-pressure offset OF (52) for the experiments shown in Fig. 12(a).

Fig. 12. Experimental results for tracking behavior of the NMPC when switching from 200 bar to 300 bar cavity-pressure reference for the virgin material.

transition are determined by the color of the ejected parts. The different phases are highlighted using white for virgin material and two different tones of blue for the two PCR batches in Fig. 13.

In the first plot, we depict the measured mass using the cycle-variant part-mass controller with $\sigma_W = 15$. For controlling the part mass, we utilized the reference shown as a red dashed line. We changed the reference m^{ref} because we reached the bounds for the cavity-pressure reference p_C^{ref}.

In the second part of Fig. 13, we depict the output of the cycle-variant part-mass controller ($\sigma_W = 15$). We also visualize the cavity-pressure reference, which would have been proposed by a part-mass controller with a cycle-invariant model ($\sigma_W = 0$). Initially, there is no notable difference between the two controller outputs until the transition to recycled material becomes apparent ($c = 22$). In contrast to the cycle-variant controller, the cycle-invariant controller shows a slower reduction in cavity-pressure reference. During cycles 25 to 27, a substantial change in the output of the cycle-invariant part-mass controller ($\sigma_W = 0$) occurs. For the same cycles, a strong decrease in the length scales determined by the hyperparameter optimization can also be observed in the third plot of Fig. 13.

The highest deviation between the part mass m and the desired part mass m^{ref} occurs when transitioning from virgin material to PCR batch E. Here, a relative deviation of almost 1 % is reached. During the processing of the PCR material, we observe higher oscillations in the measured mass compared to the virgin material. Overall, we observe a mean mass deviation of 0.21 % when transitioning between three different materials in 50 injection molding cycles.

9. Discussion

9.1. Learning from a P controller did not suffice to initialize the NMPC

The learning-enabled algorithm can learn an underlying model of the process controller using a simple plate geometry, as shown in Fig. 7, from a single process cycle carried out using a P controller. The second NMPC generation (2: NMPC) already shows a reasonable controller performance. However, the first generation of the cavity-pressure controller (1: NMPC) exhibits strong overshoots regarding the reference, along with oscillations in the cavity pressure. This is particularly evident in the left part of Fig. 9.

The controller's performance of the first NMPC generation is unacceptable and could potentially damage the injection molding machine, requiring a smoother learning process. The poor performance of the controller in the first generation is likely due to the model's limited ability to generalize between experiments conducted with a P controller and those performed with an NMPC.

One solution may be to blend the outputs of the NMPC and the P controller smoothly. It may also be beneficial to consider using a confidence measure obtained during model optimization to weigh the output of the P controller against that of the NMPC.

Furthermore, no stability guarantees can be given when switching from the P controller to the NMPC. Therefore, further research is needed to ensure a stable transition between the two controllers.

While the introduced model achieves acceptable NMPC performance, the geometry described in Section 7 is simpler than typical industrial applications. Assuming a constant $\dot{S}$ may hinder learning for more complex mold geometries, potentially deteriorating the NMPC tracking performance. However, $\dot{S}$ was deliberately chosen as a scalar value to mitigate the risk of overfitting when learning from a single injection molding experiment. Future model extensions could approximate $\dot{S}$ over time using basis functions, as for the bulk modulus. To support this increased model complexity without overfitting, incorporating additional physical constraints or training the model on data from multiple experiments would likely be required. Alternatively, a lumped thermodynamic state could be incorporated into the state vector.

9.2. NMPC was able to compensate for changes in processed material properties

Substantial differences in the screw antechamber pressure p_S are observed during the transition between virgin material and PCR in Fig. 10, while the cavity pressure remains largely unchanged, indicating a successful model adaptation. In Fig. 11, we can observe that the bulk modulus for virgin material ($c = 14$) rises earlier. The reason for that could be that the MFR for virgin material is higher, as shown in Table 1,

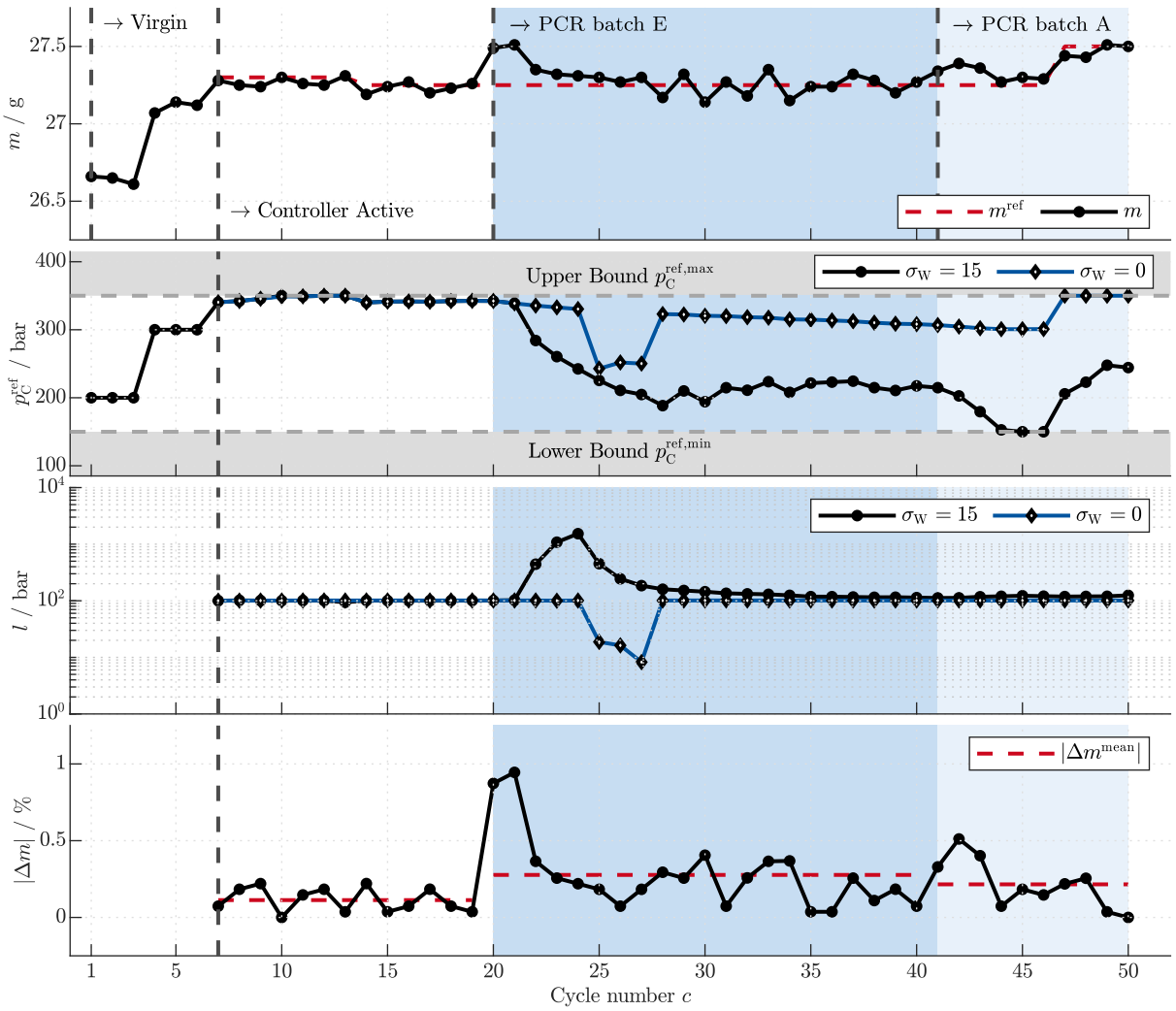

Fig. 13. Experimental results of the complete control loop, including the part-mass controller, shown over injection molding cycles c. In this experiment, we transition from virgin material to PCR batch E to PCR batch A. The first six experiments are used to identify the relationship between $p_{\mathrm{C}}^{\mathrm{ref}}$ and m when using virgin material. After each cycle, the model is updated. At $c = 20$, ejected parts show the influence of PCR batch E (determined by color). After cycle 41, the effects of the PCR batch A could be observed (determined by color).

indicating a lower viscosity and, consequently, a lower screw pressure and a higher Q_{C} with constant Q_{S}. Therefore, the point of complete cavity filling is reached at a lower ΔV_{S} value than for PCR. However, the estimated bulk modulus is twice as high for PCR as for virgin material, which seems unrealistic. This suggests that changes in viscosity are implicitly captured within this parameter as well.

In our experiments, we demonstrated that a learning-enabled NMPC can compensate for changes in material properties between polymer batches and achieve good closed-loop control performance. The model optimizer adapted the underlying model from cycle to cycle, thereby mitigating the effects of polymer batch changes.

When switching between different material batches, we would expect C_2 to change. Since this parameter is not optimized in this work, and the parameter is highly nonlinear and difficult to optimize, setting reasonable and tight bounds for this parameter could be beneficial. Alternatively, in future work a more robust identification algorithm could be examined. In this work, the model parameters were updated by using the last cycle. Using more than one cycle could also be beneficial to make the optimized model more reliable. The assumption that the drive can be adequately approximated by a first-order lag element is valid only for electric drives actuated in a moderate manner. Highly dynamic machine-operation strategies could also violate this assumption, requiring a more detailed drive modeling.

9.3. NMPC exhibited good cavity-pressure reference tracking behavior between PCR batches

Generalizing across different pressure levels is considerably easier than transitioning from a P controller to an NMPC. However, as seen in Fig. 12(a), the rise time reduces for the subsequent cycles after switching from 200 bar to 300 bar cavity-pressure reference. This effect is also visible in the RMSE. The static offset varies from cycle to cycle, which can cause problems for the part-mass controller. The part-mass controller assumes that the cavity pressure follows its reference perfectly or at least with a cycle-invariant offset. Therefore, any change in offset between cavity pressure and its reference can result in variations in part mass. This effect occurs even when the cavity-pressure reference remains constant.

The effect of the cavity-pressure offset on the quality-attribute-prediction model can be mitigated by either informing the part-mass controller of the offset or by adapting the NMPC model during the cycle, e.g., by extending the EKF from Section 5 to include an error state. Due to the model's cycle-to-cycle variability in prediction quality, the Extended Kalman Filter (EKF) is currently tuned to rely almost exclusively on measurement data. Without active denoising and an error-state formulation, the filter serves as a neutral component, neither strictly necessary nor detrimental to the controller's performance.

Future research could improve this by dynamically adapting q_{EKF} based on a measure of the model's accuracy

9.4. Part-mass controller compensated for fluctuations between PCR batches

The part-mass controller in Fig. 13 demonstrates reasonable tracking performance when transitioning between different materials. The response of the cycle-invariant part-mass controller shows that a cycle-variant kernel function is needed to calculate cavity-pressure references when transitioning between materials. The cycle-invariant controller reduces the cavity pressure too slowly, because it assigns equal weight to all observations. During cycle 25 to 27 in Fig. 13, the output of the cycle-invariant part-mass controller ($\sigma_{\mathrm{W}} = 0$) jumps to a lower level. The optimized length scales l in the third plot of Fig. 13 reveal that the cycle-invariant model starts to overfit at this point. This indicates problems in finding suitable hyperparameters for the cycle-variant observations.

One advantage of a model-based part-mass controller over a model-free approach is that it can run in an open-loop manner. The model can be updated whenever new information is available, and it does not require a fixed sample time. Since calculating the next cavity-pressure reference involves solving an optimization problem, one can choose a cost function that considers more than just the deviation between the expected and desired mass.

One major disadvantage is the high computational cost of order $\mathcal{O}(c^3)$ compared to other algorithms. Retraining the model is computationally expensive, because exact inference requires computing the inverse of the positive semi-definite covariance matrix [29]. Given the process's natural cycle times, the additional computational complexity of Bayesian inference is feasible. Should the dataset become prohibitively large, a suitable data-forgetting strategy can be applied without substantial loss of accuracy, since older observations already receive decreasing weights due to our cycle-variant kernel function. Since we switch between different materials, kernel functions other than a Wiener covariance function might be more suitable. Assuming that k decreases continuously between a new and older observation might not adequately capture an almost discontinuous event, such as transitioning between different batches of material. Ideally, k would approach zero between observations from different batches. To achieve this, a reliable detection method for different material batches is necessary.

In practice, the model-based part-mass controller can effectively compensate for batch-to-batch fluctuations. For this to work, measurements of the part mass must be available. Experiments indicate that a cycle-variant kernel function may be beneficial for transitioning between virgin material and different batches of PCR while maintaining acceptable performance. However, because the part-mass controller operates between injection-molding cycles, it cannot respond to changes in material properties during the cycle. In industrial applications, materials naturally mix within the barrel and hopper, making abrupt material transitions uncommon. However, should a sudden change occur, the mass of the molded part may fall outside acceptable tolerance ranges. Fundamentally, without a priori knowledge of the exact material properties entering the process, it is unclear how a transient deviation from the part-mass reference can be entirely avoided.

Although this study utilizes a constant cavity-pressure reference, time-varying reference trajectories can be realized by extending the input feature dimension of the GPR model. An example of utilizing such parameterized, time-varying reference trajectories is given in [16]. However, it must be noted that using multiple parameters increases the complexity of the identification problem. A higher-dimensional feature space inherently requires more injection molding cycles to train a meaningful and robust surrogate model.

10. Conclusion

We presented a learning-enabled NMPC algorithm, combined with a learning-based quality-attribute controller, applied to the injection molding process using PCR material. The results demonstrate the strong potential of the approach to compensate for batch-to-batch fluctuations and the resulting variations in part quality. Initializing the model with a P controller requires gentler blending to avoid mechanical damage.

Future work will involve validating this approach on more complex mold geometries and evaluating other quality attributes, such as gloss and dimensional accuracy. Because controlling multiple quality attributes simultaneously cannot be achieved solely by adjusting the cavity-pressure reference, subsequent studies should focus on automatically adjusting additional variables, such as mold temperature, barrel temperature, and maximum screw speed. Notably, the proposed NMPC framework already allows cycle-to-cycle adjustments to the maximum screw speed, which is incorporated as a constraint in the NMPC formulation. Furthermore, since quality attributes in injection molding are correlated, they can be efficiently represented using Multi-Output GPs, which also model their correlations [35]. These output correlations could also be leveraged to infer quality attributes that are difficult to measure, using easily accessible ones (e.g., part mass). Since adding additional inputs to GP models requires more extensive system identification, a promising approach is to integrate existing quality-attribute models as priors within the GP. Such multi-output regression models could then be used inside a multi-objective optimization.

CRediT authorship contribution statement

Jens Ahlers: Writing – original draft, Visualization, Validation, Software, Methodology, Investigation, Formal analysis, Data curation, Conceptualization. **Robert Göllinger:** Writing – original draft, Visualization, Validation, Software, Methodology, Investigation, Formal analysis, Data curation, Conceptualization. **Moritz Mascher:** Writing – review & editing, Resources, Conceptualization. **Christopher Schulte:** Writing – review & editing, Software, Conceptualization. **Philipp Schubert:** Writing – review & editing, Writing – original draft, Conceptualization. **Christian Hopmann:** Writing – review & editing, Supervision, Resources, Project administration, Funding acquisition. **Heike Vallery:** Writing – review & editing, Supervision. **Sebastian Stemmler:** Writing – review & editing, Supervision, Project administration, Funding acquisition, Conceptualization.

Funding statement

The presented research was funded by the Deutsche Forschungsgemeinschaft (DFG, German Research Foundation), Germany under the funding code 378417139 (Phasenübergreifende Prozessführungskonzepte beim Spritzgießen unter Nutzung moderner Regelungsstrategien).

Declaration of competing interest

The authors declare that they have no known competing financial interests or personal relationships that could have appeared to influence the work reported in this paper.

Acknowledgments

The authors thank Arburg GmbH & Co. KG, (Loßburg, Germany), Sabic Deutschland GmbH & Co. KG (Düsseldorf, Germany) and Systec GmbH (Köln, Germany), who provided machines and materials.

Data availability

The research data has been included in the accompanying co-publication [34].

References

[1] E. Baur, T.A. Osswald, N.S. Rudolph, Plastics Handbook: The Resource for Plastics Engineers, fifth ed., Hanser publications, Cincinnati, 2019, http://dx.doi.org/10.3139/9781569905609.

[2] R. Geyer, Production, use, and fate of synthetic polymers, in: Plastic Waste and Recycling, Elsevier, 2020, pp. 13–32, http://dx.doi.org/10.1016/B978-0-12-817880-5.00002-5.

[3] European Commission, The European Green Deal, Communication 640 final, European Commision, Brussels, Belgium, 2019, pp. 1–24.

[4] R. Dahlmann, C. Hopmann (Eds.), Nachhaltige Kunststoffverpackungen aus Post Consumer-Rezyklaten: Recyclingfähiges Design, Fertigung und Ökobilanzierung, in: SDG - Forschung, Konzepte, Lösungsansätze zur Nachhaltigkeit, Springer Fachmedien Wiesbaden, Wiesbaden, 2025, http://dx.doi.org/10.1007/978-3-658-48211-4.

[5] C. Hopmann, M. Schmitz, Plastics Industry 4.0: Potentials and Applications in Plastics Technology, Carl Hanser Verlag, Munich, 2021, http://dx.doi.org/10.3139/9781569907979.fm.

[6] P.-W. Huang, H.-S. Peng, Number of times recycled and its effect on the recyclability, fluidity and tensile properties of polypropylene injection molded parts, Sustainability 13 (19) (2021) 11085, http://dx.doi.org/10.3390/su131911085.

[7] K. Hornberg, C. Hopmann, The switchover challenge and its consequences, Kunststoffe Int. 2020 (03) (2020) 82–86.

[8] C. Bielenberg, M. Stommel, P. Karlinger, From manual to automated: Exploring the evolution of switchover methods in injection molding processes—A review, Polymers 17 (8) (2025) 1096, http://dx.doi.org/10.3390/polym17081096.

[9] K. Hornberg, Phasenübergreifende Regelung des Werkzeuginnendrucks zur Erhöhung der Reproduzierbarkeit im Spritzgießen, in: IKV - Berichte Aus der Kunststoffverarbeitung, RWTH Aachen University, Aachen, 2024, http://dx.doi.org/10.18154/RWTH-2025-00095.

[10] R. Schiffers, S. Moser, S. Kruppa, M. Busl, Verfahren Zur Bestimmung Eines Realen Volumens Einer Spritzgießfähigen Masse in Einem Spritzgießprozess, 2017.

[11] Engel GmbH, Compensation of fluctuations in plastic viscosity, 2025, Engel GmbH.

[12] J. Maderthaner, A. Kugi, W. Kemmetmüller, Optimal control of the part mass for the injection molding process, J. Process Control 129 (2023) 103027, http://dx.doi.org/10.1016/j.jprocont.2023.103027.

[13] J. Gim, E. Han, B. Rhee, W. Friesenbichler, D.P. Gruber, Causes of the gloss transition defect on high-gloss injection-molded surfaces, Polymers 12 (9) (2020) 2100, http://dx.doi.org/10.3390/polym12092100.

[14] M. Vukovic, S. Stemmler, K. Hornberg, D. Abel, C. Hopmann, Adaptive model-based predictive control for cross-phase cavity pressure control in injection molding, J. Manuf. Process. 77 (2022) 730–742, http://dx.doi.org/10.1016/j.jmapro.2022.02.030.

[15] M. Vukovic, S. Stemmler, D. Abel, K. Hornberg, C. Hopmann, A comparison of two sigma point Kalman filters for adaptive cross-phase cavity pressure control in injection molding, IFAC-PapersOnLine 55 (10) (2022) 1416–1422, http://dx.doi.org/10.1016/j.ifacol.2022.09.589.

[16] S. Stemmler, M. Vukovic, M. Ay, J. Heinisch, Y. Lockner, D. Abel, C. Hopmann, Quality control in injection molding based on norm-optimal iterative learning cavity pressure control, IFAC-PapersOnLine 53 (2) (2020) 10380–10387, http://dx.doi.org/10.1016/j.ifacol.2020.12.2777.

[17] J. Lu, Z. Cao, C. Zhao, F. Gao, *110thanniversary:* An overview on learning-based model predictive control for batch processes, Ind. Eng. Chem. Res. 58 (37) (2019) 17164–17173, http://dx.doi.org/10.1021/acs.iecr.9b02370.

[18] L. Wang, W. Zhang, Q. Zhang, H. Shi, R. Zhang, F. Gao, Terminal constrained robust hybrid iterative learning model predictive control for complex time-delayed batch processes, Nonlinear Anal. Hybrid Syst. 47 (2023) 101276, http://dx.doi.org/10.1016/j.nahs.2022.101276.

[19] L. Wang, H. Li, H. Li, R. Zhang, F. Gao, Constrained model predictive fault-tolerant control for nonlinear batch processes with time delay by integrating a LRF method and a switching strategy, Chem. Eng. Sci. 287 (2024) 119762, http://dx.doi.org/10.1016/j.ces.2024.119762.

[20] S. Horváth, J.G. Kovács, Real-time product weight estimation based on internal pressure monitoring in injection molding, Polym. Eng. Sci. 65 (4) (2025) 1693–1701, http://dx.doi.org/10.1002/pen.27078.

[21] J. Maderthaner, A. Kugi, W. Kemmetmüller, Part mass estimation strategy for injection molding machines, IFAC-PapersOnLine 53 (2) (2020) 10366–10371, http://dx.doi.org/10.1016/j.ifacol.2020.12.2775.

[22] J. Krantz, Z. Nieduzak, J. Licata, S. O'Meara, P. Gao, D. Masato, In-mold rheology and automated process control for injection molding of recycled polypropylene, Polym. Eng. Sci. 64 (9) (2024) 4112–4127, http://dx.doi.org/10.1002/pen.26836.

[23] J. Krantz, J. Licata, M.A. Raju, P. Gao, R. Ma, D. Masato, Machine learning-based process control for injection molding of recycled polypropylene, Polymers 17 (7) (2025) 940, http://dx.doi.org/10.3390/polym17070940.

[24] C. Jaroschek, Spritzgießen Für Praktiker, 2nd Auflage ed., Hanser Verlag, München, 2008, http://dx.doi.org/10.3139/9783446418066.

[25] C. Froehlich, W. Kemmetmüller, A. Kugi, Control-oriented modeling of servo-pump driven injection molding machines in the filling and packing phase, Math. Comput. Model. Dyn. Syst. 24 (5) (2018) 451–474, http://dx.doi.org/10.1080/13873954.2018.1481870.

[26] T. Albin Rajasingham, Nonlinear model predictive control of combustion engines: from fundamentals to applications, in: Advances in Industrial Control, Springer International Publishing, Cham, 2021, http://dx.doi.org/10.1007/978-3-030-68010-7.

[27] L. Schmitt, N. Nickig, M. Bahr, S. Gößling, D. Abel, Review, evaluation and application of condensing algorithms for model predictive control based on a first-order method, in: 2023 European Control Conference, ECC, 2023, pp. 1–7, http://dx.doi.org/10.23919/ECC57647.2023.10178157.

[28] C.E. Rasmussen, C.K.I. Williams, Gaussian processes for machine learning, 3rd print ed., in: Adaptive Computation and Machine Learning, MIT Press, Cambridge, Mass., 2008, http://dx.doi.org/10.7551/mitpress/3206.001.0001.

[29] D. Duvenaud, Automatic Model Construction with Gaussian Processes (Ph.D. thesis), Apollo - University of Cambridge Repository, 2014, http://dx.doi.org/10.17863/CAM.14087.

[30] P. Brunzema, A. Rohr, S. Trimpe, On controller tuning with time-varying Bayesian optimization, in: 2022 IEEE 61st Conference on Decision and Control, CDC, IEEE, 2022, pp. 4046–4052, http://dx.doi.org/10.1109/cdc51059.2022.9992649.

[31] MATLAB, 2024, The MathWorks Inc., Natick, Massachusetts, United States.

[32] K. Hornberg, C. Hopmann, M. Vukovic, S. Stemmler, D. Abel, Compensation of batch fluctuations of post-consumer recyclate in injection molding by phase-unifying process control, in: SPE ANTEC 2023, Curran Associates, Inc., Denver, USA, 2023, pp. 137–143.

[33] J.A.E. Andersson, J. Gillis, G. Horn, J.B. Rawlings, M. Diehl, Casadi: A software framework for nonlinear optimization and optimal control, Math. Program. Comput. 11 (1) (2019) 1–36, http://dx.doi.org/10.1007/s12532-018-0139-4.

[34] J. Ahlers, R. Göllinger, M. Mascher, Injection molding process data for post-consumer recycled materials, 2025, URL https://doi.org/10.18154/RWTH-2025-06809.

[35] E.V. Bonilla, K. Chai, C. Williams, Multi-task Gaussian process prediction, in: J. Platt, D. Koller, Y. Singer, S. Roweis (Eds.), Advances in Neural Information Processing Systems, Vol. 20, Curran Associates, Inc., 2007, p. 6.